Available online at www.sciencedirect.com
SCIENCE DIRECT®
Journal of Solid State Chemistry 178 (2005) 3420–3425
JOURNAL OF SOLID STATE CHEMISTRY
www.elsevier.com/locate/jssc

Ternary lithium stannides $Li_xT_3Sn_{7-x}$ (T = Rh, Ir)

Puravankara Sreeraj, Daniel Kurowski, Rolf-Dieter Hoffmann, Zhiyun Wu, Rainer Pöttgen*

Institut für Anorganische und Analytische Chemie, NRW Graduate School of Chemistry, and Sonderforschungsbereich 458, Universität Münster, Corrensstraße 30, 48149 Münster, Germany

Received 15 July 2005; received in revised form 15 August 2005; accepted 27 August 2005
Available online 3 October 2005

Abstract

The ternary stannides $Li_xRh_3Sn_{7-x}$ ($x = 0.45$, 0.64, 0.80) and $Li_xIr_3Sn_{7-x}$ ($x = 0.62$ and 0.66) were synthesized from the elements in sealed tantalum tubes in a water-cooled sample chamber of an induction furnace. The samples were characterized by X-ray diffraction on powders and single crystals. The stannides adopt the cubic Ir_3Ge_7-type structure (space group $Im\bar{3}m$, $Z = 4$). In this structure type the tin atoms occupy the Wyckoff positions 12*d* and 16*f* and form two interpenetrating frameworks consisting of cubes and square antiprisms. The rhodium and iridium atoms center the square antiprisms and are arranged in pairs. With increasing lithium substitution the lattice parameter of Ir_3Sn_7 (936.7) decreases via 932.2 pm ($x = 0.62$) to 931.2 pm ($x = 0.66$), while the Ir–Ir distance remains almost the same (290 pm). A similar trend is observed for the rhodium compounds. The lithium atoms substitute Sn on both framework sites. However, the 16*f* site shows a substantially larger preference for Li occupation. This is in contrast to the isotypic magnesium based compounds.

Keywords: Intermetallics; Crystal structure; Chemical bonding; Tin

1. Introduction

The stannides Ru_3Sn_7 [1–3], Os_3Sn_7 [4,5], $OsIr_2Sn_7$ [6], Ir_3Sn_7 [6–8], and $Ir_3In_3Sn_4$ [6] crystallize with the cubic Ir_3Ge_7-type structure [9], space group $Im\bar{3}m$, $Z = 4$. The transition metal (T) atoms have a square-antiprismatic tin coordination and two of these square antiprisms share a common square face, leading to a T_2Sn_{12} unit as the central structural motif (Fig. 1). These T_2Sn_{12} units are condensed via the tin atoms, thus forming two independent interpenetrating networks (Fig. 2).

Chemical bonding in the whole family of Ir_3Ge_7-type intermetallics has recently been investigated in detail [10]. Depending on the elements and the electron count, there is an interplay between strong *d–p* bonding for compounds of the early transition metals with group 15 or 16 elements, while combinations of the late transition metals with group 13 elements reveal completely filled *d* bands and strong *p–p* bonding within the *p*-block atom framework.

The early work by Hulliger [6] already showed solid solutions for the Ir_3Ge_7-type stannides on the transition metal as well as on the *p*-element sites. In view of the similar chemical potentials, the Os/Ir and Sn/In mixing in $OsIr_2Sn_7$ and $Ir_3In_3Sn_4$ [6] could have been expected. Our recent phase analytical investigation in the magnesium–transition metal–tin systems revealed the series of ternary stannides $Mg_xRh_3Sn_{7-x}$ ($x = 0.98-1.55$) [11] and $Mg_xIr_3Sn_{7-x}$ ($x = 0.61-1.67$) [8]. These are remarkable results in view of the non-existence of binary Rh_3Sn_7. Chemical bonding analysis for the $Mg_xIr_3Sn_{7-x}$ series revealed a decrease of the Ir–Sn (*d–p* bonding) and Sn–Sn (*p–p* bonding) interactions, when tin is substituted by magnesium. Similar substitution patterns have now been observed during our phase analytical investigations of various Li–*T*–Sn systems [12–15]. The synthesis and structural investigations of $Li_xRh_3Sn_{7-x}$ ($x = 0.45$, 0.64, 0.80) and $Li_xIr_3Sn_{7-x}$ ($x = 0.62$ and 0.66) are reported herein.

*Corresponding author. Fax: +49 251 83 36002.
E-mail address: pottgen@uni-muenster.de (R. Pöttgen).

0022-4596/$ - see front matter © 2005 Elsevier Inc. All rights reserved.
doi:10.1016/j.jssc.2005.08.021

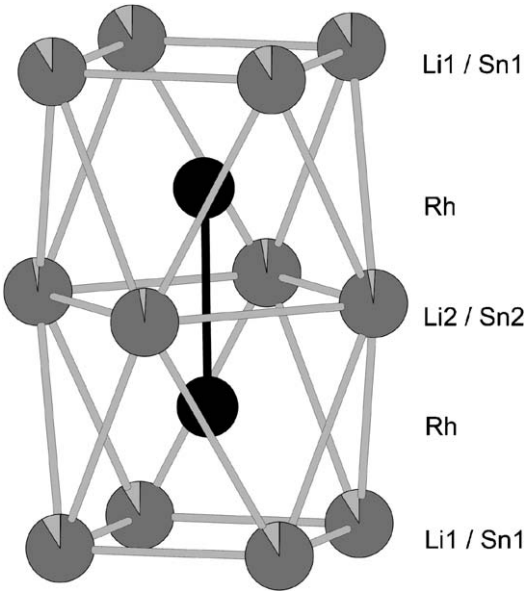

Fig. 1. The monomeric building unit in the cubic crystal structure of $Li_xT_3Sn_{7-x}$ (T = Rh, Ir). The transition metal and tin atoms are drawn as black and light gray circles, respectively. The sectors of the tin sites correspond to the different lithium content. The values presented in this drawing correspond to $Li_{0.45}Rh_3Sn_{6.55}$.

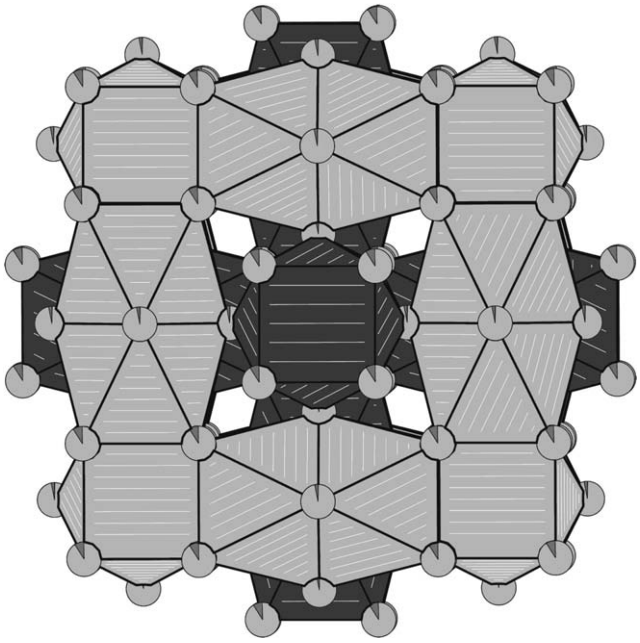

Fig. 2. The two interpenetrating networks in the structures of $Li_xT_3Sn_{7-x}$ (T = Rh, Ir). The tin atoms are drawn as light gray circles. The sectors of the tin sites correspond to the different lithium content. The values presented in this drawing correspond to $Li_{0.45}Rh_3Sn_{6.55}$.

2. Experimental

2.1. Synthesis

Starting materials for the synthesis of $Li_xRh_3Sn_{7-x}$ and $Li_xIr_3Sn_{7-x}$ were lithium rods (Merck, >99%), rhodium and iridium powder (Degussa-Hüls, 200 mesh, >99.9%), and a tin bar (Heraeus, 99.9%). For synthesizing ternary $Li_xT_3Sn_{7-x}$ stannides, the lithium rods were first cut into smaller pieces under dry paraffin oil and subsequently washed with *n*-hexane. The paraffin oil and *n*-hexane were dried over sodium wire. The lithium pieces were kept in Schlenk tubes under argon prior to the reactions. Argon was purified over a titanium sponge (900 K), silica gel, and molecular sieves.

Pieces of the lithium rods, rhodium, respectively iridium powder, and pieces of the tin bar have been weighed in the atomic ratios between x Li:3T:7−x Sn (x = 0.5, 1, 1.5, and 2). The elements were sealed in small tantalum tubes under an argon pressure of about 600 mbar [16]. The ampoules were placed in a water-cooled quartz sample chamber [17] of a high-frequency furnace (Hüttinger Elektronik, Freiburg, Typ TIG 1.5/300). In a first step, the tubes were rapidly heated under flowing argon up to 1220 K, kept at that temperature for 5 min, cooled within 10 min to 1020 K, annealed at that temperature for 2 h, and finally quenched by switching off the high-frequency generator. The temperature was controlled through a Sensor Therm Metis MS09 pyrometer with an accuracy of ±30 K.

After cooling to room temperature, the samples could easily be separated from the tantalum tubes. No reaction of the samples with the crucible material could be detected. The samples are stable in air over several weeks. Single crystals exhibit metallic luster.

2.2. EDX-analysis

The single crystals investigated on the diffractometers have been analyzed with a Leica 420 I scanning electron microscope. The EDX analyses were carried out with elemental rhodium, iridium, and tin as standards. Neither metallic impurities nor tantalum contaminants from the crucible were detected. The T:Sn ratios determined by EDX and the structure refinements agreed well, e.g. 1:2.09 from EDX and 1:2.12 from X-ray data for $Li_{0.64}Rh_3Sn_{6.36}$. Nevertheless, an uncertainty arises from the irregular surfaces of the crystals and thus, quantitative results could not be obtained from EDX.

2.3. X-ray powder data

The samples were characterized through Guinier powder diffractograms using Cu$K\alpha_1$ radiation and α-quartz (a = 491.30, c = 540.46 pm) as an internal standard. The Guinier camera was equipped with an imaging plate detector (Fujifilm, Basread-1800). The lattice parameters were obtained from least-squares fits of the powder data. To ensure correct indexing, the experimental patterns were compared to calculated ones [18], taking the atomic positions from the structure refinements. The lattice parameters determined from the powders and the single crystals showed small discrepancies, most likely due to the homogeneity ranges. The powder values were

Table 1
Crystal data and structure refinement of $Li_xRh_3Sn_{7-x}$ (space group $Im\bar{3}m$; $Z = 4$)

Empirical formula	$Li_{0.45(1)}Rh_3Sn_{6.55(1)}$	$Li_{0.64(1)}Rh_3Sn_{6.36(1)}$	$Li_{0.80(1)}Rh_3Sn_{6.20(1)}$
Formula weight	1089.27	1067.76	1050.72
Unit cell dimensions (pm)	$a = 930.91(6)$	$a = 929.09(11)$	$a = 927.31(11)$
(Single crystal data) (nm^3)	$V = 0.8067$	$V = 0.8020$	$V = 0.7974$
Calculated density (g/cm^3)	8.97	8.84	8.75
Crystal size (μm^3)	$30 \times 40 \times 60$	$20 \times 20 \times 80$	$20 \times 40 \times 60$
Detector distance (mm)	—	60	60
Exposure time (min)	—	12	30
ω range; increment (deg)	—	0–180; 1.0	0–180; 1.0
Integr. param. A, B, EMS	—	13.0; 3.0; 0.014	13.5; 3.5; 0.014
Transm. ratio (max/min)	1.19	1.75	1.32
Absorption coefficient (mm^{-1})	25.8	25.3	25.0
$F(000)$	1855	1819	1791
θ range for data collection (deg)	3–30	3–35	3–35
Range in $h\,k\,l$	± 13; $0 < k < 13$; $-13 < l < 2$	± 14; ± 14; ± 14	± 14; ± 14; ± 14
Total no. of reflections	1521	6072	5996
Independent reflections	145 ($R_{int} = 0.0293$)	204 ($R_{int} = 0.0360$)	201 ($R_{int} = 0.0317$)
Reflections with $I > 2\sigma(I)$	136 ($R_{sigma} = 0.0114$)	196 ($R_{sigma} = 0.0108$)	199 ($R_{sigma} = 0.0068$)
Data/parameters	145/12	204/12	201/12
Goodness-of-fit on F^2	1.322	1.282	1.337
Final R indices [$I > 2\sigma(I)$]	$R_1 = 0.0135$	$R_1 = 0.0288$	$R_1 = 0.0355$
	$wR_2 = 0.0197$	$wR_2 = 0.0495$	$wR_2 = 0.0710$
R indices (all data)	$R_1 = 0.0154$	$R_1 = 0.0301$	$R_1 = 0.0361$
	$wR_2 = 0.0200$	$wR_2 = 0.0499$	$wR_2 = 0.0712$
Extinction coefficient	0.00084(3)	0.0019(1)	0.0010(2)
Largest diff. peak and hole	0.56 and $-0.94\,e/Å^3$	1.92 and $-4.49\,e/Å^3$	2.07 and $-2.46\,e/Å^3$

$a = 930.1(1)$ pm for the sample 1Li:3Rh:6Sn, $a = 928.7(1)$ pm for 2Li:3Rh:5Sn, $a = 933.02(7)$ pm for 0.5Li:3Ir:6.5Sn, and $a = 933.56(9)$ for 1.0Li:3Ir:6.0Sn. Considering the degree of Sn/Li substitution, the lattice parameters of the lithium-based samples are slightly smaller than those of the magnesium-based series [8,11]. In agreement with the single crystal data discussed below, the lattice parameters of both series decrease with increasing lithium content.

2.4. Single crystal X-ray diffraction

Small, irregularly shaped single crystals of the $Li_xT_3Sn_{7-x}$ stannides were examined by use of a Buerger camera equipped with an image plate system (Fujifilm BAS–1800) in order to establish suitability for intensity data collection. Single crystal intensity data of $Li_{0.45}Rh_3Sn_{6.55}$, $Li_{0.62}Ir_3Sn_{6.38}$, and $Li_{0.66}Ir_3Sn_{6.34}$ were collected at room temperature by use of a four-circle diffractometer (CAD4) with graphite monochromatized Mo $K\alpha$ (71.073 pm) radiation and a scintillation counter with pulse height discrimination. The scans were taken in the $\omega/2\theta$ mode and empirical absorption corrections were applied on the basis of psi-scan data, followed by a spherical absorption correction. The $Li_{0.64}Rh_3Sn_{6.36}$ and $Li_{0.80}Rh_3Sn_{6.20}$ data sets were collected at room temperature using of a Stoe IPDS-II image plate diffractometer in oscillation mode. The absorption corrections were numerical. All relevant details concerning the data collections are listed in Tables 1 and 2.

Analysis of the diffractometer data sets revealed body-centered cubic cells for all stannides and space group $Im\bar{3}m$ was found to be correct during the structure refinements in agreement with the previous investigations on the magnesium based compounds [8,11]. The atomic parameters of Ir_3Sn_7 [8] were taken as starting values and the structures were refined using SHELXL-97 [19] (full-matrix least-squares on F^2) with anisotropic atomic displacement parameters for all atoms. In the first stage of the refinement we assumed the ideal T_3Sn_7 compositions. These refinements readily revealed somewhat elevated displacement parameters for the tin sites, indicating smaller scattering power on these sites. This was confirmed through refinement of the occupancy parameters of the tin sites. In parallel to the series of $Mg_xRh_3Sn_{7-x}$ and $Mg_xIr_3Sn_{7-x}$ stannides [8,11], we have subsequently refined the tin sites with a mixed Sn/Li occupancy, leading to the refined compositions $Li_xRh_3Sn_{7-x}$ ($x = 0.45$, 0.64, 0.80) and $Li_xIr_3Sn_{7-x}$ ($x = 0.62$ and 0.66) for the single crystals investigated. In the last cycles these occupancy parameters have been refined as a least-squares variable. The 12d Sn2 sites show only a minor lithium occupancy. Nevertheless, considering the standard deviations, the Sn2/Li2 substitution is significant. The final difference Fourier syntheses were flat (Tables 1 and 2). The positional parameters and interatomic distances of the refinements are listed in Tables 3 and 4. Further details on the structure refinements are available.[1]

[1]Details may be obtained from: Fachinformationszentrum Karlsruhe, D-76344 Eggenstein-Leopoldshafen (Germany), by quoting the Registry Nos. CSD–415604 ($Li_{0.45}Rh_3Sn_{6.55}$), CSD–415602 ($Li_{0.64}Rh_3Sn_{6.36}$), CSD–415603 ($Li_{0.80}Rh_3Sn_{6.20}$), CSD–415605 ($Li_{0.62}Ir_3Sn_{6.38}$), and CSD–415606 ($Li_{0.66}Ir_3Sn_{6.34}$).

Table 2
Crystal data and structure refinement of $Li_{0.62}Ir_3Sn_{6.38}$ and $Li_{0.66}Ir_3Sn_{6.34}$ (space group $Im\bar{3}m$; $Z = 4$)

Empirical formula	$Li_{0.62(1)}Ir_3Sn_{6.38(1)}$	$Li_{0.66(1)}Ir_3Sn_{6.34(1)}$
Formula weight	1338.54	1332.84
Unit cell dimensions (pm)	$a = 932.21(6)$	$a = 931.16(6)$
(Single crystal data) (nm^3)	$V = 0.8101$	$V = 0.8074(9)$
Calculated density (g/cm^3)	10.97	10.97
Crystal size (μm^3)	$20 \times 30 \times 40$	$40 \times 50 \times 70$
Transm. ratio (max/min)	2.97	1.47
Absorption coefficient (mm^{-1})	68.3	68.4
$F(0\,0\,0)$	2208	2199
θ range for data collection (deg)	3–35	3–30
Range in $h\,k\,l$	± 14; ± 14; ± 14	± 13; ± 13; $+13$
Total no. of reflections	9071	2502
Independent reflections	207 ($R_{int} = 0.0998$)	145 ($R_{int} = 0.1540$)
Reflections with $I > 2\sigma(I)$	199 ($R_{sigma} = 0.0213$)	110 ($R_{sigma} = 0.0390$)
Data/parameters	207/12	145/12
Goodness-of-fit on F^2	1.189	1.129
Final R indices [$I > 2\sigma(I)$]	$R_1 = 0.0177$	$R_1 = 0.0295$
	$wR_2 = 0.0356$	$wR_2 = 0.0524$
R indices (all data)	$R_1 = 0.0193$	$R_1 = 0.0554$
	$wR_2 = 0.0361$	$wR_2 = 0.0615$
Extinction coefficient	0.0026(1)	0.00040(6)
Largest diff. peak and hole	2.13 and $-2.07\,e/Å^3$	3.15 and $-2.54\,e/Å^3$

Table 3
Atomic parameters and equivalent isotropic displacement parameters (pm^2) of different $Li_xT_3Sn_{7-x}$ stannides (space group $Im\bar{3}m$)

Atom	Wyckoff position	Occupancy[a]	x	y	z	U_{eq}
$Li_{0.45}Rh_3Sn_{6.55}$						
Rh	12*e*	1.00(1)	0.34525(6)	0	0	87(2)
Sn1/Li1	16*f*	91.3(3)/8.7(3)	0.16335(3)	*x*	*x*	128(2)
Sn2/Li2	12*d*	96.6(4)/3.4(4)	1/4	0	1/2	109(2)
$Li_{0.64}Rh_3Sn_{6.36}$						
Rh	12*e*	1.00(1)	0.34593(10)	0	0	93(3)
Sn1/Li1	16*f*	86.9(7)/13.1(7)	0.16291(6)	*x*	*x*	141(3)
Sn2/Li2	12*d*	96.0(8)/4.0(8)	1/4	0	1/2	114(3)
$Li_{0.80}Rh_3Sn_{6.20}$						
Rh	12*e*	1.00(1)	0.34646(14)	0	0	112(4)
Sn1/Li1	16*f*	82.4(8)/17.6(8)	0.16209(9)	*x*	*x*	185(4)
Sn2/Li2	12*d*	96.9(11)/3.1(11)	1/4	0	1/2	139(3)
$Li_{0.62}Ir_3Sn_{6.38}$						
Ir	12*e*	1.00(1)	0.34465(4)	0	0	57(1)
Sn1/Li1	16*f*	86.0(5)/14.0(5)	0.16270(5)	*x*	*x*	126(3)
Sn2/Li2	12*d*	98.1(4)/1.9(4)	1/4	0	1/2	84(2)
$Li_{0.66}Ir_3Sn_{6.34}$						
Ir	12*e*	1.00(1)	0.34448(14)	0	0	84(4)
Sn1/Li1	16*f*	86.5(13)/13.5(13)	0.16241(17)	*x*	*x*	156(9)
Sn2/Li2	12*d*	97.7(14)/2.3(14)	1/4	0	1/2	109(7)

[a]Occupancy parameters of the Rh (Ir) positions of $Li_xT_3Sn_{7-x}$ (T = Rh, Ir) were obtained in separate series of least-squares cycles. In the final cycles the ideal occupancy values were assumed for these sites. The Li1/Sn1 and Li2/Sn2 occupancies were refined as least-squares variables for all $Li_xT_3Sn_{7-x}$ stannides.

3. Results and discussion

The stannides $Li_xRh_3Sn_{7-x}$ ($x = 0.45$, 0.64, 0.80) and $Li_xIr_3Sn_{7-x}$ ($x = 0.62$ and 0.66) with cubic Ir_3Ge_7-type structure (space group $Im\bar{3}m$) [9] have been synthesized and structurally characterized. The transition metal atoms are located at the position 12*e* ($x00$) and the Li/Sn atoms occupy the sites 16*f* (xxx) (Li1/Sn1) and 12*e* ($\frac{1}{4}0\frac{1}{2}$) (Li2/Sn2). The degree of tin/lithium substitution increases with increasing x of $Li_xT_3Sn_{7-x}$ for the starting composi-

Table 4
Interatomic distances in the stannides $Li_xT_3Sn_{7-x}$. All distances <400 pm are listed (standard deviations in parentheses)

	$Li_{0.45}Rh_3Sn_{6.55}$	$Li_{0.64}Rh_3Sn_{6.36}$	$Li_{0.80}Rh_3Sn_{6.20}$	Ir_3Sn_7	$Li_{0.62}Ir_3Sn_{6.38}$	$Li_{0.66}Ir_3Sn_{6.34}$
T						
4 *M*1	273.7(1)	272.8(1)	272.1(1)	274.4(1)	273.5(1)	272.9(1)
4 *M*2	273.7(1)	273.4(1)	272.8(1)	276.2(1)	274.4(1)	274.2(1)
1 *T*	288.8(1)	286.3(2)	284.8(3)	294.1(1)	289.7(1)	289.6(3)
*M*1						
3 *T*	273.7(1)	273.4(1)	272.8(1)	274.4(1)	273.5(1)	272.9(1)
1 *M*1	279.4(1)	280.3(2)	282.4(3)	275.4(2)	281.9(1)	282.5(6)
3 *M*1	304.1(1)	302.7(1)	300.6(2)	308.7(1)	303.3(1)	302.5(3)
6 *M*2	357.6(1)	357.1(1)	357.0(1)	358.2(1)	358.5(1)	358.2(1)
*M*2						
4 *T*	273.7(1)	272.8(1)	272.1(1)	276.2(1)	274.4(1)	274.2(1)
4 *M*2	329.1(1)	328.5(1)	327.9(1)	330.7(1)	329.6(1)	329.2(1)
8 *M*1	357.6(1)	357.1(1)	357.0(1)	358.2(1)	358.5(1)	358.2(1)

M denotes Li/Sn mixing. The data of Ir_3Sn_7 [8] are listed for comparison.

tion. Since the crystal chemistry and chemical bonding of Ir_3Ge_7-type intermetallics have already been discussed in detail [1–11], herein, we focus only on the structural and chemical bonding peculiarities of $Li_xT_3Sn_{7-x}$ and a comparison with the $Mg_xRh_3Sn_{7-x}$ and $Mg_xIr_3Sn_{7-x}$ stannides [8,11]. One main difference between the $Li_xT_3Sn_{7-x}$ and $Mg_xT_3Sn_{7-x}$ stannides is the degree of tin substitution which is significantly smaller for the lithium based series. The values of $x = 0.80$ and 0.66 seem to be the limits of the solid solutions $Li_xRh_3Sn_{7-x}$ and $Li_xIr_3Sn_{7-x}$. X-ray powder patterns of samples with higher lithium content already showed the stannides $LiRh_3Sn_5$ [20], $LiRhSn_4$ [21,22], or $LiIrSn_4$ [21,22] as additional phases.

The transition metal atoms in $Li_xT_3Sn_{7-x}$ have a square-antiprismatic lithium/tin coordination. Two of these square-antiprisms are condensed via a common square face forming the basic building unit (Fig. 1). These double prisms are aligned on each edge of the cubic unit cell. Thus, six double-prisms form a cube around each corner of the cell. The size of the cube is determined by the *x* parameter of the Li1/Sn1 positions. As emphasized in Fig. 2, the complete structure consists of two interpenetrating frameworks which share the Li2/Sn2 atoms, a consequence of the body-centered lattice.

The refined positional parameters of the $Li_xT_3Sn_{7-x}$ stannides can be compared to those of Ir_3Sn_7 [8] and the series $Mg_xRh_3Sn_{7-x}$ [11]. The *x* parameter of iridium increases from 0.34278 (Ir_3Sn_7) to 0.34465 in $Li_{0.62}Ir_3Sn_{6.38}$, leading to shorter (290 pm) Ir–Ir distances as compared to Ir_3Sn_7 (294 pm). The Ir–Ir distances are even slightly shorter than in the $Mg_xIr_3Sn_{7-x}$ series [8]. The *x* parameter of rhodium in $Li_{0.80}Rh_3Sn_{6.20}$ (0.34646) is comparable to $Mg_{1.55}Rh_3Sn_{5.45}$ (0.3452) [11], resulting in almost similar Rh–Rh distances of 285 and 288 pm, respectively.

The most significant difference between the series of $Li_xT_3Sn_{7-x}$ and $Mg_xT_3Sn_{7-x}$ intermetallics is the kind and degree of tin substitution. In both magnesium-based series, the 12*d* Sn2 positions always have a much higher degree of tin substitution, while the 16*f* Sn1 site in the $Li_xT_3Sn_{7-x}$ stannides has the significantly higher lithium content. This is most likely a geometric effect. The smaller lithium atoms (123 and 136 pm covalent radius for Li and Mg [23], respectively) seem to favor the 16*f* site with the shorter *M*1–*M*1 distances, while the magnesium atoms in the $Mg_xT_3Sn_{7-x}$ series favor the 12*d* site with the longer *M*2–*M*2 distances (Table 4).

The largest difference to the binary Ir_3Sn_7 structure [8] occurs for the *x* parameter of the Sn1/Li1 (*M*1) site which is 0.16241 as compared to 0.16500 for Ir_3Sn_7. This leads to somewhat different interatomic distances: 275.4 (1*x*) and 308.7 pm (3*x*) Sn1–Sn1 in Ir_3Sn_7 as compared to 282.5 (1*x*) and 302.5 pm (3*x*) *M*1–*M*1 in $Li_{0.66}Ir_3Sn_{6.34}$. For a detailed description of the chemical bonding peculiarities of the magnesium-based solid solution $Mg_xIr_3Sn_{7-x}$ we refer to [8].

Finally we wish to comment on the unexpected tin/lithium substitution. Although our recent investigations on binary transition metal indides and stannides revealed substantial indium/magnesium and tin/magnesium substitution [8,11,24,25, and refs. therein], only few examples with lithium exist. So far, only the series $Li_{3-x}Pt_2Sn_{3+x}$ [26] and $Li_{1+x}Pd_2Sn_{6-x}$ [27] have been reported. More recently indium/lithium substitution has also been observed for $K_{34}In_{92.30}Li_{12.70}$ and $K_{14}Na_{20}In_{91.82}Li_{13.18}$ [28]. In view of the diagonal similarities in the periodic table (similarities between lithium and magnesium), the tin/lithium substitution is not unreasonable, given the fact that many tin/magnesium substitutions exist.

Acknowledgments

We are grateful to the Degussa-Hüls AG for a generous gift of rhodium and iridium powder and to B. Heying and Dipl.-Ing. U. Ch. Rodewald for the intensity data collections. This work was supported by the Deutsche

Forschungsgemeinschaft through Sonderforschungsbereich 458 "*Ionenbewegung in Materialien mit ungeordneten Strukturen*". P.S. is indebted to the NRW Graduate School of Chemistry for a Ph.D. stipend.

References

[1] O. Nial, Sven. Kem. Tidskr. 59 (1947) 172.
[2] B.C. Chakoumakos, D. Mandrus, J. Alloys Compd. 281 (1998) 157.
[3] L. Eriksson, J. Lanner, Acta Crystallogr. E57 (2001) i85.
[4] N.V. Kalyaeva, S.V. Popova, Neorg. Mater. 19 (1983) 997.
[5] B. Künnen, D. Niepmann, W. Jeitschko, J. Alloys Compd. 309 (2000) 1.
[6] F. Hulliger, Nature 209 (1966) 500.
[7] O. Nial, Sven. Kem. Tidskr. 59 (1947) 165.
[8] M. Schlüter, U. Häussermann, B. Heying, R. Pöttgen, J. Solid State Chem. 173 (2003) 418.
[9] K. Schubert, H. Pfisterer, Z. Metallkd. 41 (1950) 433.
[10] U. Häussermann, M. Elding-Pontén, C. Svensson, S. Lidin, Chem. Eur. J. 4 (1998) 1007.
[11] M. Schlüter, A. Kunst, R. Pöttgen, Z. Anorg. Allg. Chem. 628 (2002) 2641.
[12] R. Pöttgen, Zh. Wu, R.-D. Hoffmann, G. Kotzyba, H. Trill, J. Senker, D. Johrendt, B.D. Mosel, H. Eckert, Heteroatom Chem. 13 (2002) 506.
[13] Zh. Wu, R.-D. Hoffmann, D. Johrendt, B.D. Mosel, H. Eckert, R. Pöttgen, J. Mater. Chem. 13 (2003) 2561.
[14] Zh. Wu, B.D. Mosel, H. Eckert, R.-D. Hoffmann, R. Pöttgen, Chem. Eur. J. 10 (2004) 1558.
[15] P. Sreeraj, R.-D. Hoffmann, Zh. Wu, R. Pöttgen, U. Häussermann, Chem. Mater. 17 (2005) 911.
[16] R. Pöttgen, T. Gulden, A. Simon, GIT Labor-Fachz. 43 (1999) 133.
[17] D. Kußmann, R.-D. Hoffmann, R. Pöttgen, Z. Anorg. Allg. Chem. 624 (1998) 1727.
[18] K. Yvon, W. Jeitschko, E. Parthé, J. Appl. Crystallogr. 10 (1977) 73.
[19] G.M. Sheldrick, SHELXL-97, Program for Crystal Structure Refinement, University of Göttingen, 1997.
[20] P. Sreeraj, D. Johrendt, H. Müller, R.-D. Hoffmann, Zh. Wu,, R. Pöttgen, Z. Naturforsch. 60b (2005) 933.
[21] Zh. Wu, R.-D. Hoffmann, R. Pöttgen, Z. Anorg. Allg. Chem. 628 (2002) 1484.
[22] Zh. Wu, H. Eckert, J. Senker, D. Johrendt, G. Kotzyba, B.D. Mosel, H. Trill, R.-D. Hoffmann, R. Pöttgen, J. Phys. Chem. B 107 (2003) 1943.
[23] J. Emsley, The Elements, Clarendon Press, Oxford, 1989.
[24] V. Hlukhyy, R. Pöttgen, J. Solid State Chem. 177 (2004) 1646.
[25] V. Hlukhyy, R. Pöttgen, J. Solid State Chem. 178 (2005) 79.
[26] R.-D. Hoffmann, Zh. Wu, R. Pöttgen, Eur. J. Inorg. Chem. (2003) 3425.
[27] P. Sreeraj, R.-D. Hoffmann, Zh. Wu, R. Pöttgen, U. Häussermann, Chem. Mater. 17 (2005) 911.
[28] B. Li, J.D. Corbett, J. Am. Chem. Soc. 127 (2005) 926.